Ferroelectricity and chirality in the $Pb_5Ge_3O_{11}$ crystal

Mauro Fava [1,*] William Lafargue-Dit-Hauret [1,2] Aldo H. Romero [3] and Eric Bousquet [1]

[1] *Physique Théorique des Matériaux, QMAT, CESAM, Université de Liège, B-4000 Sart-Tilman, Belgium*

[2] *Universite de Pau et des Pays de l'Adour, E2S UPPA, CNRS, IPREM, Pau, France*

[3] *Department of Physics and Astronomy, West Virginia University, Morgantown, West Virginia 26505-6315, USA*

(Received 20 November 2023; revised 10 January 2024; accepted 11 January 2024; published 26 January 2024)

We study from first-principles calculations the ferroelectric structural phase transition of $Pb_5Ge_3O_{11}$ crystal. The calculations of phonons and Born effective charges of the paraelectric phase allow us to identify a polar instability that is unstable in both transverse-optic and longitudinal-optic versions, giving rise to an entire branch of instability along a propagation vector parallel to the mode polarization (the hexagonal axe). This is the hint of hyperferroelectricity and the stable head-to-head and tail-to-tail domain, as recently reported from both experiments and theory. Then, our analysis of the ferroelectric phase shows that the polarization of $Pb_5Ge_3O_{11}$ is uniaxial along the hexagonal axes and with small in-plane components due to a piezoelectric effect. The symmetry-adapted mode analysis shows that the total ferroelectric ground-state distortion comes mainly from polar distortions of the unstable polar phonon mode but also from an invariant, cooperative mode that amplifies the polar deformation. We also build a phenomenological model that highlights how the coupling between these modes is at play and helps us understand how to reproduce the second-order phase transition. Lastly, we also quantify the structural chirality through the continuous symmetry measure method and trace its origin to the polar unstable mode itself. By extending our approach to the phonon states, we further show that the chirality is poorly affected by the relaxation but could also be enhanced by activating high-frequency modes with polar symmetry. Finally, we study the phonon angular momentum (AM) distribution in both phases and identify trends in the AM behavior across the Brillouin zone.

DOI: 10.1103/PhysRevB.109.024113

I. INTRODUCTION

Synthesis of the compound lead germanate $Pb_5Ge_3O_{11}$ (PGO) dates back to 1971 [1,2]. Subsequent experimental works [3] have established the main features of PGO, among which is the existence of a high-temperature amorphous structure ($T > 618$ K), an intermediate temperature hexagonal paraelectric (PE) phase ($450\ K < T < 618\ K$) with $P\bar{6}$ symmetry and a low-temperature ferroelectric (FE) phase ($T < 450$ K) with the trigonal $P3$ space group. The presence of a hysteresis loop for the natural optical activity, i.e., gyroelectricity [4,5], in the $P3$ FE phase, mirroring the one of the detected polar order, was also found in those early studies [3,6], implying opposite handedness for the $+P$ and $-P$ states. Additionally, a sequence of experimental works on PGO have focused on the dielectric response, structural and ferroic properties [3,7–13], on the piezoelectricity [14], pyroelectricity [15–19], and the electro-optical properties [20–23]. Measurements of the spontaneous polarization as a function of temperature reveal a uniaxial polarization along the hexagonal axis and the second-order character of the FE phase transition. The presence of a hysteresis loop in the natural optical activity measurements can be associated with the *gyrotropic* order associated with the $P3$ space group [24,25], which can indeed be associated with optically active polar domains. Furthermore, the linear electrogyration [4] coefficient of PGO is among the largest ever recorded, with a value $\gamma_{33} = (3.1 \pm 0.3) \times 10^{-11}$ m/V near 450 K in chromium doped conditions (0.8%) [25–28]. Another intriguing aspect of PGO involves its FE domain walls (DWs). Notably, the material has been observed to exhibit the phenomenon of topological bifurcation, as discussed in previous research [29,30]. Additionally, recent experimental findings have identified the presence of antiferroelectric DWs [31]. These unconventional behaviors in PGO's DWs present a compelling case for further investigation, mainly through theoretical explanations grounded in first-principles calculations.

While the past five decades have seen considerable experimental work on PGO, theoretical investigations have been mainly confined to mean-field modeling to fit experimental data and only three recent exceptions employed density functional theory (DFT) [31–33]. In this paper, we investigate the microscopic mechanisms driving PGO's phase transitions with the help of *ab initio* calculations. The paper is organized as follows. After reporting our technical details for the calculations and method of analysis and the structural information of PGO, we first analyze the PE $P\bar{6}$ phase through density functional perturbation theory (DFPT). The resulting calculations of phonon dispersion curves and Born effective charges help us to identify a single unstable polar phonon branch where both the transverse and longitudinal optical (respectively, TO and LO) cases are unstable, emphasizing the hyperferroelectric [34] character of the polar phase and the soft mode origin of the phase transition. In

*mfava@uliege.be

the next section, we scrutinize and characterize the FE $P3$ phase with DFT and DFPT. The use of symmetry adapted mode (SAM) decomposition of the distortions present in the $P3$ phase helps us to identify the relevant modes at play in the phase transition. Then we build a phenomenological model to describe the energy landscape involving these modes that helps us to understand the role of the spin orbit coupling (SOC) to reproduce the second-order phase transition. Finally, we extend our analysis to quantify the chirality of the $P3$ phase and the associated phonon modes by employing the continuous symmetry measures technique [35]. This rigorous approach enables us to pinpoint the origin of chirality within PGO and elucidates the underlying reasons for its gyroelectric properties. We argue that the chirality of this material is not associated with a phonon angular momentum (AM), contrary to that observed in recent works [36,37]. The further exploration of the AM shows values close to 1 Ha for some bands in the FE phase and a trend of the PE and FE AM distributions with respect to the phonon wave vector. Our findings not only shed light on the intrinsic chiral nature of the $P3$ phase but also provide a deeper understanding of the gyroelectric behavior exhibited by PGO, thereby contributing to the broader comprehension of symmetry-breaking phenomena in FE materials.

II. TECHNICAL DETAILS

Structural relaxations, energy, and response function calculations have been performed with the DFT code ABINIT v9.6.2 [38,39] and through norm-conserving pseudopotentials from the PseudoDojo project [40] (v0.4). The generalized gradient approximation with the Perdew-Burke-Ernzerhof functional for solids (PBEsol) [41] was used. A $3 \times 3 \times 3$ k-point grid and a cutoff of 50 Ha (1360.57 eV) were employed and found sufficient to converge total energies and structural relaxation (cell parameter and atomic positions), as well as phonon frequencies. Density functional perturbation theory (DFPT) [42] response functions in both the PE and FE phases were used to obtain the phonon frequencies, the Born effective charges, and the permittivity tensor [42]. The Born effective charges and the dielectric tensor allows us to evaluate the nonanalytical dipole-dipole long-range (LR) part of the dynamical matrix [42], giving rise to the LO modes. The phonon dispersion curves were calculated by interpolating the interatomic force constants (IFCs) from the unit cell only by splitting the LR part from the rest [considered the short range (SR)]. This interpolation from the unit cell allows us to reduce the computational workload, and it is an acceptable approximation as the unit cell is already large enough (around $10 \times 10 \times 10$ Å^3) to give reasonable values for the SR part over several neighbors. The Berry phase theory [43] was employed to obtain the polarization of the FE phase. The latter is also estimated from the Born effective charges to check whether it is free from spurious quanta [44]. SOC has been included in all calculations as it appeared to have a surprisingly strong effect in PGO (see Refs. [33,45]). Finally, the group theory analysis of the structural distortions was performed by means of the AMPLIMODES software [46]. Because of the size of the system (57 atoms), we will refer the reader to the Supplemental Material (SM) [45] for extra details and data (like the Born effective charges, the full phonon dispersion and frequencies, etc.) that would weigh the main text down.

III. STRUCTURAL INFORMATION

Lead germanate is a large band-gap insulator that undergoes a structural phase transition at 450 K. It features a high-temperature hexagonal PE $P\bar{6}$ phase. In contrast, its low-symmetry FE $P3$ phase disrupts the sixfold rotoinversion and the mirror symmetry along the c axis. We detail the relaxed structural attributes of the PE and FE phases in the SM. The unit cell for both phases comprises 57 atoms, with the PE and FE phases characterized by 15 and 23 asymmetric Wyckoff positions (WPs), respectively. A schematic representation of the high-symmetry PE phase is provided in Fig. 1. In this structure, lead atoms occupy two distinct positions: those at $6l$ and $3k$ WPs form hexagonal configurations around a vacuum volume when viewed along the [001] direction. In contrast, the other lead atoms are aligned along the c axis within the bulk part of the material. Germanium atoms, in coordination with surrounding oxygens, form either GeO_4 tetrahedra or Ge_2O_7 bitetrahedra. The lead atoms serve as bridges between these germanium-oxygen units. A comparative analysis of the lattice parameters with respect to the employed DFT functional has been presented in a previous work (see the SM of Ref. [33]). It is worth noting that the PBEsol functional plus SOC used in our study slightly overestimates the a and c lattice parameters by up to 0.38% and 0.25% compared to experimental values. Hence, throughout the rest of the paper we use the PBEsol plus SOC calculations as a reference, since they provide the most accurate results compared to other functionals such as PBE [41] and LDA. In the FE phase, the $3d$ WP is occupied by all the oxygen and germanium atoms. In contrast, lead atoms are found in the $3d$, $1c$, and $1b$ positions. Interestingly, both $P\bar{6}$ and $P3$ space groups exhibit axial order and a nonzero piezoelectric tensor [47,48], less commonly observed in the PE phase of FE materials.

IV. ANALYSIS OF THE PARAELECTRIC PHASE

In this section, we analyze the $P\bar{6}$ PE phase of PGO to identify and characterize the phonon instabilities. After the complete structural relaxation, we calculated the phonon frequencies, the Born effective charges, and the permittivity at the Γ point through DFPT with and without including SOC. The irreducible representation at Γ is $30A' \oplus 27A'' \oplus 64E' \oplus 50E''$, where the A'' (Γ_2) and E' (Γ_3/Γ_5) characters are infrared (IR) active with polarization along the z and xy directions, respectively, and the A' (Γ_1) and E'' (Γ_4/Γ_6) are Raman active only. From our calculated phonons we find at Γ a single unstable TO phonon mode with a frequency $\omega_0 = 34i$ cm^{-1} and of Γ_2 representation that is an IR active mode polarized along the c axis. If we look at the difference between the TO and LO frequencies associated with this unstable mode, we realize that they are very close: $34i$ cm^{-1} for the TO mode vs 28i cm^{-1} for the LO mode. We also find that, contrary to several other structural and electronic properties (see Ref. [33] and the next sections of the present paper), the inclusion of SOC in the calculation does not influence much this unstable phonon mode frequency:

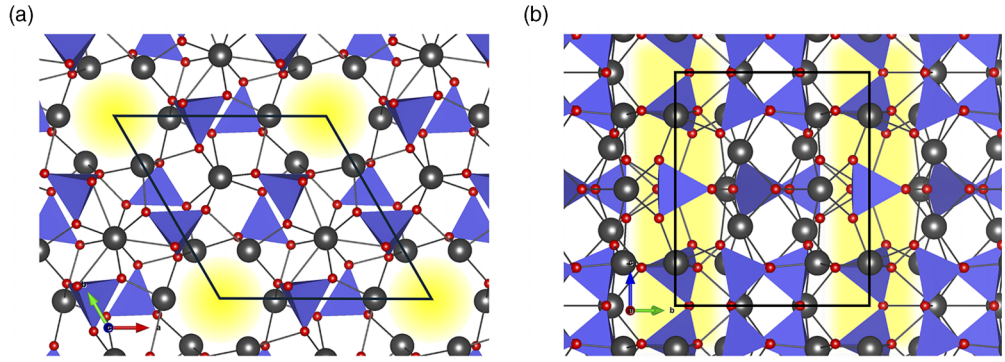

FIG. 1. (a) [001] top view and (b) [100] side view of the PE unit cell of $Pb_5Ge_3O_{11}$. Pb and O atoms are shown in dark grey and red, respectively. GeO_4 polyhedral environments are represented in purple. Empty channels are evidenced in yellow.

$\omega_{TO} = 37i\ cm^{-1}$ and $\omega_{TO} = 31i\ cm^{-1}$. Moreover, splitting the square frequencies at Γ in SR and LR contributions [42,49,50] reveals the short-range nature of the polar instability with $\omega^2_{0;SR} = -2235.2\ cm^{-1}$ and $\omega^2_{0;LR} = 1022.5\ cm^{-1}$.

Given that the unstable mode is polarized along the c axis, we aim to investigate the complete optical branch extending from the unstable Γ point to the A point, which has coordinates $(0, 0, \frac{1}{2})$. To facilitate this, we leverage the large size of the unit cell—approximately 10 Å^3 box—to interpolate the phonon dispersion solely based on dipole-dipole interactions at finite q values. The outcome of this interpolation between the Γ and A points is depicted in Fig. 2, where we have zoomed to the low-frequency part of the spectrum for clarity. The presence of a soft acoustic mode in our observations can be ascribed to the constraints of the simplified interpolation model utilized in our analysis. Our computational results uncover a comprehensive unstable phonon branch spanning the Γ to A points of the Brillouin zone, characterized by minimal

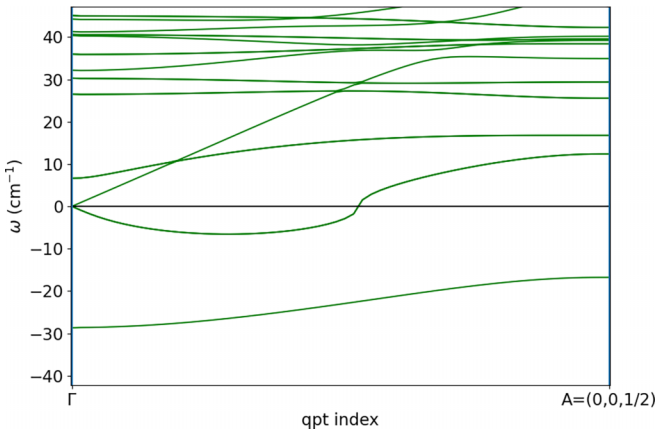

FIG. 2. Calculated phonon dispersion curves of the PE reference structure of PGO between the zone center Γ point and the zone boundary A $(0, 0, \frac{1}{2})$ points and for a zoomed frequency range between $45i$ to 45 cm^{-1}. The NAC correction has been taken into account along the (0,0,1). Hence, the unstable branch running from Γ to A corresponds to the LO polar mode at Γ associated to the unstable TO mode with Γ_2 symmetry. The unstable branch from one of the acoustic modes is an interpolation artifact as the condensation of the related elastic instability never gives a lower energy phase.

dispersion. This suggests that the model, while effective in a general sense, may not fully capture the complexities of the phonon interactions within the material, indicating the need for a more nuanced approach to accurately represent the dynamic behavior of the phonons across the entire band. To verify that this is not a spurious effect of the interpolation, we have calculated the phonons from DFPT at the A point and found a tiny deviation with respect to the purely interpolated value ($17.1i$ cm^{-1} from DFPT vs $16.8i$ cm^{-1} from dipole-dipole interpolation). Thus, it is clearly the LO mode that connects the related unstable dispersion branch along the Γ-A line.

In agreement with the calculations in Ref. [31], our results concerning the soft mode suggests that PGO behaves like a hyperferroelectric, that is, a FE crystal that can support a polarization in $\mathbf{D} = 0$ condition of the displacement field [34]. To further probe this possibility, we have computed the Born effective charges (BEC) and the electronic permitivity ε^∞ (see all the tensors in SM [45]). Even if the band gap is rather large, giving a rather small ε^∞ ($\varepsilon^\infty_{zz} = 5.1$) and even though a few BEC are anomalous (e.g., the zz BEC component of Pb at WPs $1i$ and $1e$ of around $+4e$ and at $1c$ close to $+5e$), the overall mean square value $\sqrt{\sum_{jk}(Z^\alpha_{jk})^2/57} \simeq (2.7, 2.7, 2.8)e$ is rather nominal. Hence, the Coulomb term driving the LO-TO splitting that schematically evolves as the average BEC over ε^∞ is small enough to keep the LO mode unstable [34]. Having an average BEC value close to nominal can also mean that PGO does not present an overall anomalously large charge transfer due to covalent bonds [34], unlike common FEs. We further show in the SM [45] that the SOC weakly affects the Born effective charges and ε^∞, i.e., a few percent increase. Analysis on known hyperferroelectric compounds such as $LiNbO_3$ and ABC hexagonal systems [51,52] allows us to dig deeper into the mechanism behind this SR instability. In particular, Ref. [52] shows that the SR destabilization in hyperferroelectrics ABO_3 and ABC types is coming from negative on-site IFCs. However, in the SM [45], we show that the on-site IFCs are all positive in PGO, therefore ruling out the Ref. [52] argument in the case of PGO. While we do not investigate this finding in detail, we can possibly understand it from a rigid-unit perspective as reported in, e.g., silicates [53]. In fact, one can see that both the high- and low-symmetry phases are comprised of oxygen-sharing Ge- and Pb-centered

quasirigid polyhedra. Thus, the source of the polar instability does not involve individual self-forces (due to the rigidity of the polyhedra), but is rather connected with the stabilization of oxygen-mediated nearest-neighbor interactions between these units. The instability would stay geometric but from rigid-unit motions instead of atomic origin [54].

Our calculations, hence, confirm that PGO is a FE material with a uniaxial polarization and with a proper order parameter as described by the soft mode theory [55] and as observed experimentally [56–59]. Further confirmation of a hyperferroelectric character would require finding a nonzero polarization in open circuit boundary conditions. Results supporting such conclusions are given in the next section.

V. ANALYSIS OF THE FERROELECTRIC PHASE

Given that the soft mode aligns with the symmetry of the (FE) phase, it is reasonable to classify the phase transition of PGO as a proper FE transition. We begin our analysis of the polar state with the SOC off. Starting with the PE structure as a reference, we induce a symmetry breaking by displacing ions along directions dictated by the unstable phonon eigenvector and with various amplitudes. We observe a double-well energy landscape, with energy minima corresponding to a gain of 9.0 meV/f.u. At these minima, we calculate the spontaneous polarization $\mathbf{P}_s$ and find a magnitude of 2.8 $\mu C/cm^2$ along the c axis. This value is notably smaller than the experimentally reported 5.0 $\mu C/cm^2$ [3] when extrapolated to 0 K. To reconcile this discrepancy, we first conduct a structural relaxation with fixed cell parameters and then recalculate the energy gain and polarization. The revised values are 61 meV/f.u. and 5.3 $\mu C/cm^2$, respectively. Consistently with the phonon instability, we detect no in-plane components of $\mathbf{P}_s$. A second structural optimization—in which the relaxation of the lattice parameters with respect to the PE phase is allowed—finally gives an energy gain of 68 meV/f.u. and $\mathbf{P}_s$ of 5.9 $\mu C/cm^2$ along the z direction which extrapolates correctly the experimental value. Unlike the previous cases, a small in-plane polarization $\mathbf{P}_s^{xy} = (-0.07, 0.05)$ $\mu C/cm^2$ is now observed in the fully relaxed case, which is associated with the piezoelectric nature of the high-symmetry reference structure. The Berry phase computed values of the polarization are consistent with those found from the atomic displacements and the Born effective charges. As we remind that the spin orbit has been deactivated during the calculations of the aforementioned quantities, from a previous work [33] we also know that the SOC renormalizes the FE barrier up to ∼30% of its value. In fact, the SOC increases the unrelaxed soft mode energy up to 13 meV, the ion-only relaxed energy up to 80 meV, and the fully relaxed FE ground-state energy up to 89 meV. It therefore comes naturally to understand how $\mathbf{P}_s$ is affected by the spin-orbit interaction as well. The calculation of the polarization with the SOC included gives $\mathbf{P}_s = (-0.04,\ 0.02,\ 5.5)$ $\mu C/cm^2$. Given that the energies are much affected by the SOC, having a relatively SOC independent polarization means that much of the SOC contribution affects the nonharmonic part of the energy, a fact that is also supported by the energy of the unrelaxed soft modes computed either with or without spin-orbital contribution.

The fully relaxed FE cell parameters are $a = b = 10.257$ Å and $c = 10.689$ Å and align well with experimental findings, as detailed in the SM [45]. To check whether a further symmetry lowering might occur, we recalculated the phonon frequencies at the Γ point and found no unstable mode, confirming the stability and ground state of our relaxed $P3$ phase.

Hence, we can summarize our DFT calculations as follows. Internal ion relaxation is clearly of paramount importance in reaching both the minimum energy configuration and reproducing the experimental polarization, while strain optimization has a secondary importance (the additional gain of energy when including the strain is much smaller than the gain of energy given by the internal atom relaxation alone). The role of the internal forces can be somehow expected, given the presence of both a large number of atoms (57) in the unit cell with a low symmetry site, and of Pb^{2+} cations that have 6 s -6 p lone pairs, which are known to lead to a strong relaxation effect in FE perovskite compounds like $PbTiO_3$ [60]. To further understand the PE-FE ground state distortions $|\delta\rangle$, we perform a SAM analysis. We find that the distortion is characterized by two SAMs. The main one (1.47 Å) is associated with a $P3$ isotropy subgroup and a Γ_2 irreducible representation (namely, the same as the unstable polar mode). The second SAM (0.35 Å) is instead a mode with $P\bar{6}$ space group and Γ_1 representation. This confirms that it is the Γ_2 SAM that breaks the PE symmetry and favors a polar state, while the presence of Γ_1 deformations means that the degrees of freedom already present in the $P\bar{6}$ phase (i.e., the atoms with WP that are not at high symmetry positions) change to accommodate the polar deformation.

A graphic representation of the two relevant SAMs is given in Fig. 3. In particular, the invariant mode is clearly constituted by atomic in-plane distortions, while the polar mode contains out-of-plane displacements as well. To have more details about which phonon modes contribute to the total ground-state distortion, we did a projection of the FE distortion $\langle\delta|$ into the phonon eigenvectors $|\xi_i\rangle$ obtained in the PE phase. This projection reveals that, despite the strong relaxation, the overlap coefficient $\langle\delta|M|\xi_{\text{soft}}\rangle$ of the soft mode is about 0.90. As the normalization is $\langle\xi_i|M|\xi_j\rangle = \delta_{ij}$, it means that all the other modes give a total overlap of about 0.44. Hence, the final FE distortion is close to the unstable polar mode eigendisplacement but other higher frequency mode eigendisplacements contribute too. If we now decompose $|\delta\rangle$ into atomic type, we find that O and Pb atoms are those that contribute the most to the polarization. This result strengthens a rigid unit picture of the phase transition, with $|\delta\rangle$ described by the motion of Ge-O tetrahedra [61].

With the goal of probing the energy landscape (taking again the PE structure as reference), we extract configurations corresponding to either the total $|\delta\rangle$ deformation and its Γ_1 and Γ_2 SAM projections, linearly interpolating between the high- and low-symmetry structures. Then, we performed DFT calculations as a function of the mode amplitudes. To understand the numerical results we build a simple phenomenological internal energy model with the Γ_1 and Γ_2 SAM mode distortions as order parameters of the system. Taking into account the symmetry of these two order parameters, we find (see Ref. [45] for a thorough analysis of the fit) that the

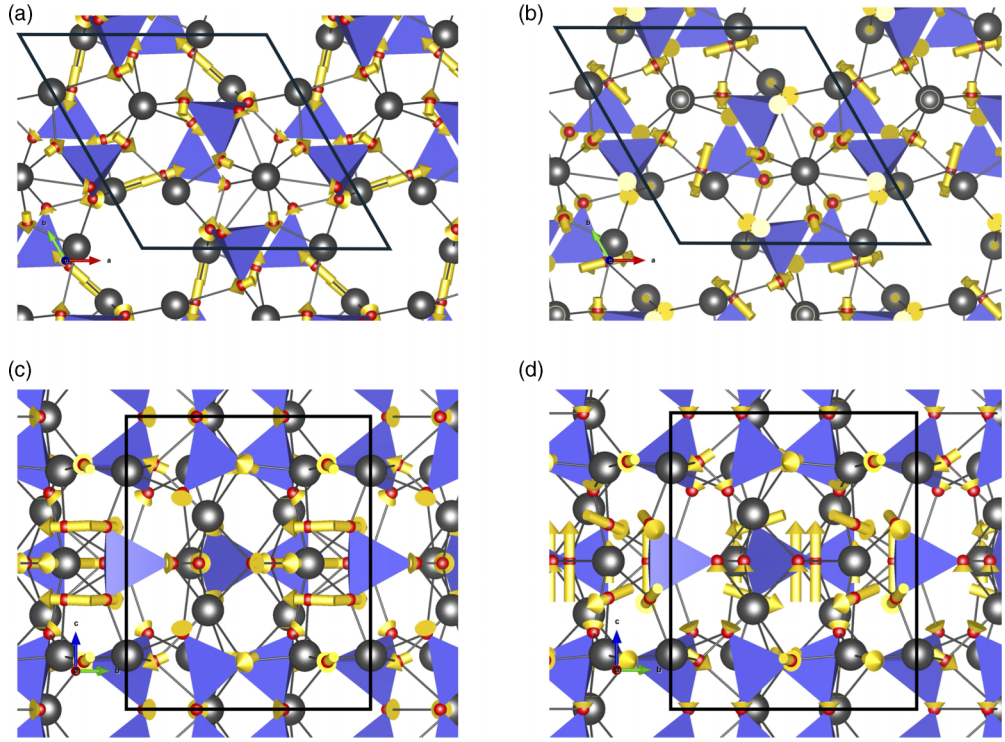

FIG. 3. (a)–(c) Top and side views for Γ_1 symmetry adapted modes (SAMs), and (b)–(d) for Γ_2 SAMs as calculated with AMPLIMODE software from our relaxed $P\bar{6}$ and $P3$ phases. The arrow lengths are proportionals to the magnitude of the distortions.

ab initio energy-configuration data set is well represented by the following expression:

$$U(Q_1, Q_2) = \frac{\alpha_1}{2}Q_1^2 + \frac{\alpha_2}{2}Q_2^2 + \frac{\beta_2}{4}Q_2^4 + aQ_1Q_2^2 + V_{\text{high}}(Q_1, Q_2), \quad (1)$$

where Q_1 and Q_2 are the amplitudes of the Γ_1 and Γ_2 distortions, respectively, and where V_{high} contains higher order terms of the expansion (see the SM [45]). Since Γ_1 is invariant under all the symmetry operations of the PE reference, it can appear in all orders (except in the first order, since the forces in the PE reference are zero). After fitting the model onto our DFT calculations, we can observe the energy wells and landscape in Fig. 4. We can see that, as expected, the Γ_1 SAM alone gives a single well around the PE reference (yellow curve) and the Γ_2 mode alone gives a double well shape (green curve). When both Γ_1 and Γ_2 are coupled together, we can observe a strong increase of the double well energy and distortion amplitude (red curve). This confirms that, in PGO, the number of internal degrees of freedom strongly enhances the development of the polar distortion into the structure, as anticipated by our previous relaxation procedure. This enhancement is mainly due to the attractive $aQ_1Q_2^2$ coupling term, which strongly renormalizes and reduces the value of the anharmonic parameter β_2. Nevertheless, our calculations also show that the reduction is not strong enough to affect the sign of the quartic Q_2^4 coefficient, which means that the phase transition remains of the second-order kind, as experimentally observed. The inclusion of higher order terms (Q_1^3, Q_2^6, $Q_1^2Q_2^2$,

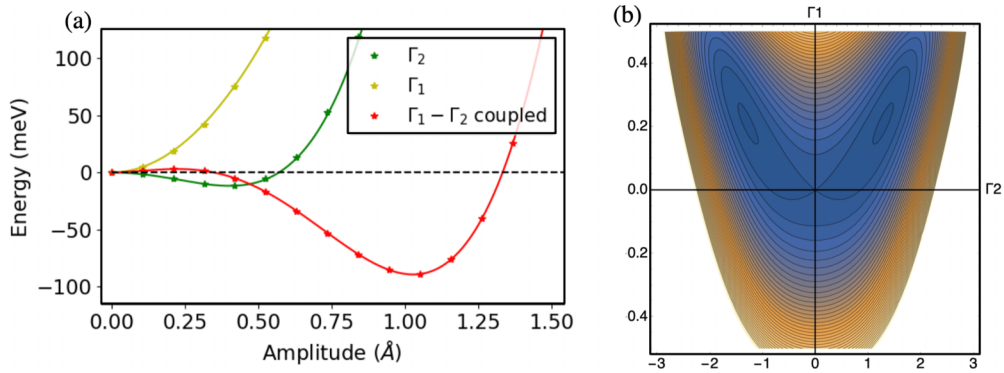

FIG. 4. Energy landscape of PGO as a function of the amplitude of the SAM Γ_1 and Γ_2. Symbols are DFT calculations while the plain lines correspond to fitted model Eq. (1). SOC is included the PE and FE structures have been fully relaxed.

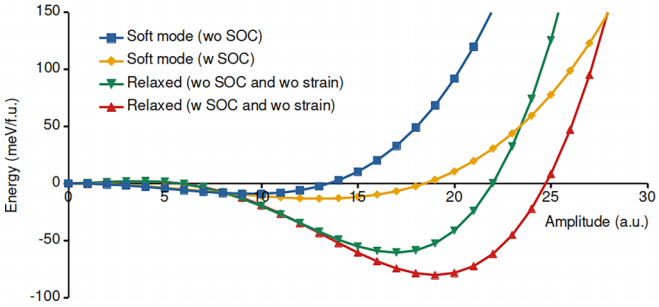

FIG. 5. Energy change versus amplitude of the polar unstable mode eigendisplacements and of the relaxed ferroelectric distortion (both at fixed cell parameter of the PE phase) with and without SOC. The zero energy reference corresponds to the PE $P\bar{6}$ phase.

$Q_1Q_2^4$, etc.) can improve the fitting for bigger values of the SAM amplitudes, but this has a quite marginal importance near the energy minimum. The strong renormalization of the FE barrier induced by the spin-orbit interaction has been anticipated by us in a previous work [33]. To highlight this effect, we show in Fig. 5 the difference in the energy wells when condensing the soft mode and the different amplitude of the fully relaxed distortion with and without SOC. We can clearly see the relevance of the SOC on the polar distortion energy landscape where it is mostly within the large atomic displacements that the SOC is at play and, hence, into the anharmonic part as observed from the phonon frequencies calculations from DFPT, which were slightly affected but the SOC.

Although we did not probe the Berry phase as a function of the SAM amplitudes, we can safely assume a linear relation $Q_2 \sim \mathbf{P}$ which is generally justified for small distortion amplitudes. Finally, we stress that although the Berry phase was calculated in $\mathbf{E} = 0$ conditions, the detection of an unstable LO branch prompts the question about what $\mathbf{P}(\mathbf{D} = 0)$ may be. This calculation from first principles is prohibitively costly in the state-of-the-art DFT code implementation, however, if we assume that the electrostatics affects only the quadratic part of the electric enthalpy, we can estimate $\mathbf{P}(\mathbf{D} = 0) \approx \mathbf{P}(\mathbf{E} = 0)\frac{\omega_{\mathrm{LO}}}{\omega_{\mathrm{TO}}} \sim 4.0\ \mu\mathrm{C/cm}^{-2}$, which is a remarkably small reduction in comparison with hyperferroelectric materials such as LiBO$_3$ (with B = V, Nb, Ta and Os) [51]. Naturally, a further decrease may be expected if non-harmonic effects are taken into account. Given that the previous linear relation actually fails even in the simpler cases of ABC hyperferroelectrics [34], we can consider the given number as an upper bound. Equivalently, the $\mathbf{D} = 0$ correction to the free energy brings an additional positive term proportional to P^2, and it can be observed that the FE instability is not suppressed as a result of the large dielectric constant of PGO. Indeed, the most prominent contribution from the electrostatic energy associated with the $\mathbf{D} = 0$ condition adds a $\mathrm{P}^2/2\epsilon$ term to the free-energy expansion (see SM [45] and Refs. [62,63] therein included), and this increases the α_2 coefficient of Eq. (1) from the value of -135.0 meV/Å to that of -119.5 meV/Å, which is compatible with hyperferroelectricity as suggested in the previous section and in agreement with the recent results reported in Ref. [31]. Our calculations also show that the effect of the SOC on the energy landscape mainly affects the anharmonic terms via ion relaxation, despite not changing the qualitative picture.

It has come to our attention that recent experimental and theoretical results [obtained through piezoresponse force microscopy (PFM) and phase-field modeling] and highlighted in Refs. [29,30] have shown the presence of charged head-to-head/tail-to-tail DWs in PGO. It has been argued that charged DWs should not form as they would be difficult to screen: this point of view has been justified on the grounds that the electronic band gap of ∼3 eV is too wide to support a total screening of the depolarization field. Moreover, while the presence of some n- or p-type doping can be expected from, e.g., vacancies in the system, both the valence band maximum (VBM) and conduction band minimum (CBM) states of PGO have been found to be localized in a recent theoretical work [33]. This electronic localization should make the screening of P_z at the DW by free charges coming from dopants even more difficult on top of the large band gap. It is thus clear that the screening originates by a different mechanism.

Following this idea, more recent PFM measurements have been explained in terms of a complex topological pattern consisting of bifurcated domains, so the interface bound charge is practically zero—namely, $\rho = \rho_z + \rho_{xy} \sim 0$ with $\rho_z = -\partial P_z/\partial z$ and $\rho_{xy} = -\partial P_x/\partial x - \partial P_y/\partial y$—which would make $\mathbf{P}$ divergenceless. In other words, if the variation of the polarization along z generates a ρ_z charge density, this would be readily compensated by the in-plane variations of P_x and P_y. However, a nonzero hyperferroelectric polarization in open circuit boundary conditions may be associated with a gap closing—as also obtained for the LiBeSb and LiNbO$_3$ compounds [64] and well-described by the simple relation $E_{\mathrm{gap}}(L) = E_{\mathrm{gap}}(0) - 2eLP(D = 0)/\epsilon$ (ϵ being the dielectric constant in the material, L the domain size, and $E_{\mathrm{gap}}(0)$ the bulk gap), thus providing for a complete screening of the depolarization field. Clearly, this is not the observed mechanism in PGO, nevertheless populating the conduction bands may still have a strong impact on the DW physics. For one thing, the FE barrier is enhanced under n-doping conditions [33]. Second, the population of the localized CBM cavity states [33] via photoexcitation or electron injection may produce an additional increase of $\partial P_z/\partial z$ assuming the $\nabla \cdot \mathbf{P} = 0$ relation to be topologically protected. This condition could potentially correspond to the realization of the antiferroelectric DWs observed under electron beams [31], despite the latter being energetically unfavorable with respect to a sharp DW.

VI. CHIRALITY MEASURE AND PHONON ANGULAR MOMENTUM

The phenomenon of gyrotropic switching in PGO has been attributed to the presence of both Ge_2O_7 and GeO_4 units within the same unit cell, a rare occurrence in crystals. Neutron diffraction [65] and high-resolution transmission electron microscopy [66] experiments support the idea that the polarization arises as a consequence of the twist of Ge_2O_7 quasi-rigid units and polar motion of Pb^{2+} cations. As the latter form a bridge between the bitetrahedra and the GeO_4 units—via Pb–O bonds—the polar instability generates a rotation of the germanate tetrahedra, which in turn plays a

fundamental role in determining the structural chirality. The Γ_2 mode can be appreciated in Fig. 3, and one can indeed see that it produces a chiral twist of the central GeO_4 elements and remove the mirror plane at $z = 0.5$.

A compelling theoretical inquiry centers on how individual phonon modes within the infrared (IR) spectrum, associated with the $P3$ isotropy group, contribute to the chirality and gyrotropic switching behavior of PGO. To offer a clearer understanding of this behavior, an appropriate metric for chirality must first be established. We stress that, contrary to what is stated in Ref. [31], the Γ_1 mode cannot be chiral since it is an invariant of a space group which contains a mirror operation. Rather, and as already mentioned, we can attribute an axial symmetry to that mode which survives the phase transition. Given that the low-symmetry phase is polar and chiral at the same time while the high-symmetry reference phase is PE and achiral, the spontaneous polarization may be a fitting metric or order parameter in this case. Therefore, one may eventually use the mode effective charges [42,67] as a means to probe the chirality of each phonon mode.

Nevertheless, to quantify chirality we adopt a more geometric approach and thus employ the definition of continuous chirality measure (CCM) proposed by Zabrodsky and Avnir [35], of which we give a short description as follows. The starting point is a chiral distribution Q of N atoms $\{q_i\}$. We define the following quantity:

$$\chi_Q(G) = 100 \times \min_{G \in S_n} \left[\frac{\sum_i |\vec{q}_i - \vec{p}_i|^2|}{\sum_i |\vec{q}_i - \vec{q}_0|^2|} \right], \tag{2}$$

where $\vec{q}_0$ is the geometric center of the reference Q structure and $\vec{p}_i$ are the unknown coordinates of a distribution P of N points with symmetry operations given by the achiral point group G (among the improper rotations S_n) of choice. The P distribution can be obtained by applying the operations of G to the Q structure, as described in Ref. [35]. The structural chirality is thus calculated by searching for the closest (distancewise) nonchiral distribution of points $P_{\min}$ which preserves the connectivity of Q and is compatible with the symmetry operations of G. Clearly, $\chi(Q) = 0$ if Q is achiral. On the other hand, $\chi(Q) = 100$ can be shown to be the maximum possible distance with respect to the nonchiral reference structure, which corresponds to the—unrealistic—case of all points of P converging to $\vec{q}_0$. It is thus realized that the CCM is conceived to quantify the geometrical chirality of a molecule without the foreknowledge of an eventual achiral phase (reachable without breaking interatomic bonds). Naturally, this is not the case of PGO: if we condense a Γ_2 mode on the PE equilibrium phase while keeping the amplitude of the deformation small, the achiral reference *must* be the original $P\bar{6}$ structure, meaning that we can simply write

$$\chi(\Gamma_2) = 100 \times \frac{\sum_j \left|\delta_j^{|e_k\rangle}\right|^2}{\sum_i (x_{i;\mathrm{FE}} - x_{\mathrm{C.o.M.;FE}})^2} \approx 100 \times \frac{\sum_j \left|\delta_j^{|e_k\rangle}\right|^2}{\sum_i (x_{i;\mathrm{PE}} - x_{\mathrm{C.o.M.;PE}})^2}, \tag{3}$$

where we assume $\delta_j^{|e_k\rangle}$ to be the Cartesian deformation of the M atom induced by the condensation of the kth polar eigendisplacement. Clearly, the previous expression can be employed for phonon modes and SAMs as well, provided that they belong to the representation with $P3$ isotropy space group. We have thus calculated χ for PGO in several relaxation conditions, with the results reported in Table I. The invariant distortion that comes with optimizing the FE structure must be subtracted to compute the CCM.

TABLE I. Chirality measure for the $P\bar{6}$ (PE) and $P3$ structures. FE (unstable) corresponds to the freezing of displacements associated to the unstable phonon mode eigendisplacement (i.e., no relaxation is done but the calculation is done at the lowest energy point); I corresponds to the ion relaxation only (i.e., the cell parameters are not relaxed and fixed to those of the $P\bar{6}$ PE reference); and I+V corresponds to the fully relaxed case of both cell parameters and ionic positions. $\chi(Q)$ and ΔE have been computed with the spin-orbit interaction on. The numbers between parentheses represent the (normalized) Euclidean distance between the two phases when the achiral Γ_1 contribution is not subtracted.

	PE	FE (unstable)	FE (I)	FE (I+V)
$\chi(\Gamma_2)$	0.0	0.03	0.04(0.14)	0.04(0.16)
$\chi(Q)$	0.0	/	0.04(0.55)	0.04(0.59)
ΔE (meV)	0.0	−13	−80	−89

We can see that the CCM of the soft eigenmode is substantially unaffected by the relaxation process, although the Euclidean distance between the two phases is about five times bigger. This is in agreement with the existence of a strong coupling between the soft and invariant modes and, at the same time, of a weak overlap between the distortion and stable eigenstates with Γ_2 representation. While the CCM of the analyzed chiral/polar mode is small, there are in total 171 phonon modes, many of which are also chiral. It is thus natural that we look at the value of χ for all the phonon modes at the Γ point.

The result is highlighted in Fig. 6, where we show the mode chirality versus phonon frequency as calculated with CCM applied on the eigendisplacement vectors. We can see

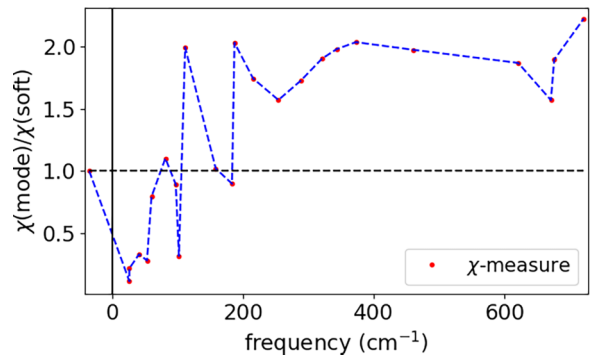

FIG. 6. Phonon mode chirality (as calculated from CCM method) as a function of the frequency (the dashed line is a guide to the eye and is at the amplitude of the unstable mode value). The soft mode value is taken as a normalization reference. Only the polar modes with Γ_2 character are considered (modes polarized along the z direction).

that several high-frequency modes have a mode chirality that is larger than the one of the unstable mode driving the phase transition ($\chi > \chi_{\text{unstable }\Gamma_2}$) while low-frequency modes have the tendency to have a smaller value. Hence, even if the unstable polar mode gives by far the largest overlap projection ($\langle\delta|M|\xi\rangle_{\text{soft}} \sim 0.9$) onto the full distortion, the small extra polar modes coefficients that are at play to completely characterize the polar deformation also possess an enhanced CCM. These strongly chiral modes are mostly associated with oxygen atom vibrations as their lower mass makes them contribute the most to high-frequency vibrations. Additionally, and with respect to Eq. (1), we can conclude that the equilibrium structural chirality of the FE phase of PGO is tight to the Q_2 amplitude and do not depend considerably on the interaction between polar and invariant SAMs, unlike the spontaneous polarization.

The high-frequency strongly chiral modes only weakly affect the behavior of the phase transition, however, it could be advisable to design nonequilibrium strategies to couple those states to the polar distortion, since it would guarantee a significant level of control on the already remarkable gyrotropic properties of PGO, with the possibility of realizing a ferrochiral memory device. Recent theoretical works have devised a mechanism based on infrared pumping to obtain fast polarization reversal in ferrodistorted perovskites [68]. A subsequent experimental verification [69] on the rhombohedral phase of $LiNbO_3$ has found only a partial (without reaching the reversed equilibrium value) and temporary switching, with the effect of the reversal being canceled after a transient. The reasons behind the incompleteness (only ∼40%) of the switching has been attributed to spatial inhomogeneities, while its cancellation—with a return to the original state after some time after the initial pump—has been explained in terms of coupling with other modes, not considered in Ref. [68], and in terms of missed relaxation along the unstable phonons orthogonal to the c axis, given the cubic nature of the high-temperature phase of the material under consideration. Chen *et al.* [70] found that it is possible to achieve a full reversal in a rhombohedral phase cooccurring with an in-plane rotation, but that seems to require a fine-tuning of the amplitude of the pulse. Thus, they have proposed the realization of a complete and permanent switching through a squeezing mechanism, with the high- and low-symmetry phases being tetragonal and orthorhombic, respectively. Assuming an initial $P_z \neq 0$, a laser pulse along the z direction is used to cancel the out-of-plane polarization and to create in-plane polar distortions (Fig. 2 of Ref. [70]). After that, three pulses (equally separated by a time lag) are applied along the a, b, and, finally, c crystal axes. The final outcome is the full and permanent reversal of P_x and P_y, while P_z remains zero (Fig. 3 of Ref. [70]). It thus appears that the xy-rotational component is a fundamental prerequisite to achieving fast polarization switching in a controllable fashion in FE perovskites. On the other hand, PGO is an uniaxial crystal and the in-plane rotation of **P** is energetically unfavored. It is, hence, possible, that a fast switching mechanism as envisioned in Ref. [68] could be more easily realized in this system.

Given the recent surge of interest concerning structural chirality in crystals [71], we provide a comparison between the kind of chirality as found in PGO and that, for instance, related to zone boundary modes as observed in several 2D and 3D systems [36,37,72] with the C_3 symmetry. The present literature on the topic thus far has been focused on circularly polarized phonon modes, which can, in fact, be triggered by photons with the same polarization [37] and produce an orbital magnetic moment as a result of their circular motion [73]. Since the threefold symmetry is associated with a pseudoangular momentum [72], selection rules ensue from its conservation. While in two dimensions the valley chirality coincides with a local circular rotation (defined per sublattice), in 3D such rotation is combined with a propagation along an axis perpendicular to the rotational plane. We further point out that 3D chiral phonons have been defined and observed in enantiomorphic crystals [36], where the direction of the circulation defines the space group and therefore a handedness [71]. Instead, at Γ the modes are static and the system has the symmetry of the point group. This means that the circular polarization of the phonons averages to zero for each mode and that a handedness cannot be defined as in the previously mentioned cases. Also, no AM [74] should be expected at zone center as a consequence of the time-reversal symmetry alone, which is confirmed for each phonon branch by our numerical calculations [45]. Due to the high number of bands, we find it more practical to analyze the distribution of the AM—the AM density of states—along the in-plane $\Gamma \rightarrow K$ (1/3,1/3,0) and out-of-plane $\Gamma \rightarrow A$ (0,0,1/2) Brillouin zone directions as shown in Fig. 7 (we report the full band-by-band computations in the SM [45]). In particular, it is clear how higher values of the AM are reached in the FE phase and, in particular, along the c direction. Moreover, values close to 1 Ha are also more frequently reached in the out-of-plane case of the FE phase. A closer inspection of the band decomposition of the AM [45] also highlights the near zone boundary (center) character of the in-plane (out-of-plane) FE distribution, with the PE bands behaving in a complementary way.

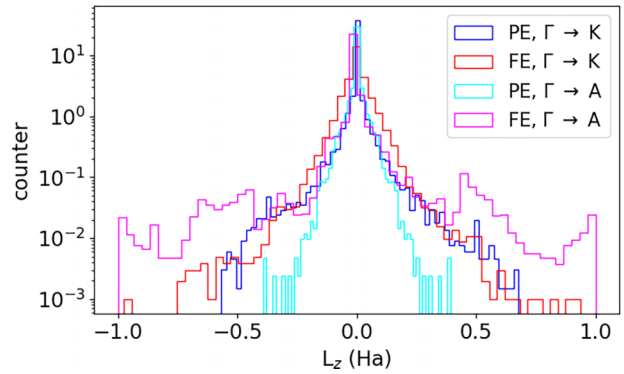

FIG. 7. Distribution (log scale) of the phonon angular momentum along the $\Gamma \rightarrow K$ and $\Gamma \rightarrow A$ directions.

Therefore, and to conclude this section, the chirality of PGO herein reported has no AM and is thus a property of the point group itself (where polar representation is axial and thus chiral as well) and is not associated with a specific handedness. As such, it can be triggered by a linearly polarized electric field and its tuning matches that of the spontaneous polarization.

VII. SUMMARY AND CONCLUSIONS

We have conducted first-principles calculations to investigate various properties and the phase transition from PE to FE states in the compound $Pb_5Ge_3O_{11}$ (PGO). Our findings illuminate the microscopic mechanisms underlying the polar deformation, pinpointing a polar mode as the primary source of instability. By calculating the Born effective charges, we establish no significant anomalous charge transfer, suggesting that geometric effects or lone pairs are more decisive factors. Our data corroborate the classification of PGO as a hyperferroelectric compound [31]. This conclusion is evidenced by the persistence of the instability even under the $\mathbf{D} = 0$ condition (i.e., after accounting for LO-TO splitting). This observation implies that domains polarized along the c axis would remain stable despite variations in boundary conditions, ranging from periodic ($\mathbf{E} = 0$) to open circuit boundary conditions ($\mathbf{D} = 0$). Furthermore, we demonstrate that the phonon branch associated with the soft mode remains unstable up to the zone boundary.

Exploring the energy landscape reveals the central role of an invariant Γ_1 and polar Γ_2 modes: their nonlinear coupling bolsters the magnitude of the polarization along the z axis and deepens the energy barrier between opposite domains. We hypothesize that this effect—remarkable despite the relatively small magnitude of the invariant distortion—may be associated with the presence of lone pairs of Pb atoms. The computed spontaneous polarization—either with the Berry phase approach or the Born effective charges—is consistent with the value found in experiments. Also, we correctly reproduce the second-order character of the phase transition.

We further discuss the behavior of DWs based on recent results that appeared in the literature [29,30]. Having an uniaxial $\mathbf{P}$ (parallel to the z axis) means that domains can meet in a charged head-to-head/tail-to-tail configuration, thus with a sizable depolarization field: normally, the fulfillment of such requirement would remove or strongly reduce the polar instability [75,76] if the DW bound charge stemming from $\partial P/\partial z$ cannot be properly screened. However, this does not seem to be the case for PGO since experiments do detect the formation of domains below the critical temperature [29–31]. Therefore, we are left with the question of how charge neutrality can be ensured and the depolarization field screened. A recent theoretical development suggests the formation of an in-plane polarization, which would neutralize the bound charge associated with the $P3$ polar phase at the interface without needing a free carrier (n-p) distribution. The resulting $\nabla \cdot \mathbf{P} = 0$ condition has a topological character and is associated with domain bifurcation, observed via PFM. We further conjecture that the topological index associated with the charge neutrality and the recently discovered conduction cavity states [33] in PGO may be used to control the DWs through the screening effect.

The spontaneous polarization of PGO also comes with a gyrotropic order, primarily associated with the tilting of the GeO_4 units concerning the high symmetry configuration. We have evaluated the chirality from CCM for the Γ_2 phonon modes and the relaxed distortions. It is found that structural optimization can increase chirality as a result of the interaction between the soft polar mode and the invariant modes. Furthermore, the calculation of the CCM associated with Γ_2 polar phonons shows the presence of high-frequency modes with a chirality χ value twice as high as the value associated with the unstable eigenstate. We argue that developing interaction with such modes (e.g., with ultrafast laser excitations [77]) could produce unique effects in the realm of polarization switching, with a potential increased level of control on the gyrotropic properties of this material and with the possibility of creating storage devices based on geometric chirality. It would also be interesting to compute from first principles [78] the optical activity associated with the phonon modes and the polar distortions to have a clearer idea of the link between chirality (as calculated through CCM) and the optical activity in PGO. We also highlight that the AM of the polar and chiral Γ_2 phonons is strictly zero, in contrast with previously reported chiral phonons that are away from zone center with nonzero AM.

Hence, PGO is a versatile material with numerous properties of high interest for multifunctional applications embedded into a single bulk material, yet not fully explored or exploited.

ACKNOWLEDGMENTS

The authors acknowledge E. McCabe, Z. Romestan, and H. Djani for fruitful discussions, and M. Vaestraete and M. Mignolet for sharing their ongoing phonon AM implementation within the ABINIT code (not yet in the production version). Computational resources have been provided by the Consortium des Équipements de Calcul Intensif (CÉCI), funded by the Fonds de la Recherche Scientifique (F.R.S.-FNRS) under Grant No. 2.5020.11 and the Tier-1 Lucia supercomputer of the Walloon Region, infrastructure funded by the Walloon Region under Grant Agreement No. 1910247. M.F. and E.B. acknowledge FNRS for support and the PDR project CHRYSALID No. 40003544. Work at West Virginia University was supported by the U.S. Department of Energy (DOE), Office of Science, Basic Energy Sciences (BES) under Award No. DE-SC0021375. This work also used Bridges2 and Expanse at Pittsburgh supercomputer center and San Diego Supercomputer Center through allocation DMR140031 from the Advanced Cyberinfrastructure Coordination Ecosystem: Services and Support (ACCESS) program, which is supported by Grants No. 2138259, No. 2138286, No. 2138307, No. 2137603, and No. 2138296.

[1] H. Iwasaki, K. Sugii, T. Yamada, and N. Niizeki, Appl. Phys. Lett. **18**, 444 (1971).
[2] S. Nanamatsu, H. Sugiyama, K. Doi, and Y. Kondo, J. Phys. Soc. Jpn. **31**, 616 (1971).
[3] H. Iwasaki, S. Miyazawa, H. Koizumi, K. Sugii, and N. Niizeki, J. Appl. Phys. **43**, 4907 (1972).
[4] K. Aizu, Phys. Rev. **133**, A1584 (1964).
[5] V. K. Wadhawan, Acta Cryst. A **35**, 629 (1979).

[6] H. Iwasaki, K. Sugii, N. Niizeki, and H. Toyoda, Ferroelectrics **3**, 157 (1972).

[7] R. Newnham, R. Wolfe, and C. Darlington, J. Solid State Chem. **6**, 378 (1973).

[8] M. I. Kay, R. E. Newnham, and R. W. Wolfe, Ferroelectrics **9**, 1 (1975).

[9] G. R. Barsch, L. J. Bonczar, and R. E. Newnham, Physica Status Solidi A **29**, 241 (1975).

[10] J. L. Kirk, L. E. Cross, and J. P. Dougherty, Ferroelectrics **11**, 439 (1976).

[11] A. Mansingh, K. N. Srivastava, and B. Singh, J. Appl. Phys. **50**, 4319 (1979).

[12] Y. N. Venevtsev, A. A. Bush, A. Y. Shashkov, V. V. Chechkin, N. P. Gertsen, S. Y. Stefanovich, and N. V. Rannev, Ferroelectrics **38**, 785 (1981).

[13] Y. Shaldin, A. Bush, S. Matyjasik, and M. Rabadanov, Crystallogr. Rep. **50**, 836 (2005).

[14] T. Yamada, H. Iwasaki, and N. Niizeki, J. Appl. Phys. **43**, 771 (1972).

[15] W. K. Zwicker, J. P. Dougherty, M. Delfino, and J. Ladell, Ferroelectrics **11**, 347 (1976).

[16] G. A. Bordovskii, V. A. Izvozchikov, V. T. Avanesyan, V. A. Bordovskii, and K. L. Kozhevnikov, Ferroelectrics **18**, 109 (1978).

[17] K. Takahashi, H. Ueda, T. Suzuki, and K. Kakegawa, Ferroelectrics **154**, 41 (1994).

[18] S. A. Fadnavis and A. G. Katpatal, Ferroelectrics **211**, 79 (1998).

[19] A. Wazalwar and A. Katpatal, Mater. Lett. **55**, 221 (2002).

[20] N. Uchida, T. Saku, H. Iwasaki, and K. Onuki, J. Appl. Phys. **43**, 4933 (1972).

[21] V. M. Bichard, P. H. Davies, K. F. Hulme, G. R. Jones, and D. S. Robertson, J. Phys. D: Appl. Phys. **5**, 2124 (1972).

[22] W. A. Nordland, Ferroelectrics **5**, 287 (1973).

[23] R. C. Miller, W. A. Nordland, and A. A. Ballman, Ferroelectrics **7**, 109 (1974).

[24] C. Konak, V. Kopsky, and F. Smutny, J. Phys. C: Solid State Phys. **11**, 2493 (1978).

[25] O. G. Vlokh, Ferroelectrics **75**, 119 (1987).

[26] I. S. Zheludev, Soviet Physics Uspekhi **19**, 1029 (1976).

[27] Č. Koňák, J. Fousek, and H. D. Kürsten, Ferroelectrics **21**, 347 (1978).

[28] Y. Uesu, N. Okada, and Y. Fukushima, J. Phys.: Condens. Matter **3**, 3377 (1991).

[29] O. Bak, T. S. Holstad, Y. Tan, H. Lu, D. M. Evans, K. A. Hunnestad, B. Wang, J. P. V. McConville, P. Becker, L. Bohatý, I. Lukyanchuk, V. M. Vinokur, A. T. J. van Helvoort, J. M. Gregg, L.-Q. Chen, D. Meier, and A. Gruverman, Adv. Funct. Mater. **30**, 2000284 (2020).

[30] Y. Tikhonov, J. R. Maguire, C. J. McCluskey, J. P. V. McConville, A. Kumar, H. Lu, D. Meier, A. Razumnaya, J. M. Gregg, A. Gruverman, V. M. Vinokur, and I. Luk'yanchuk, Adv. Mater. **34**, 2203028 (2022).

[31] M. Conroy, D. R. Småbråten, C. Ophus, K. Shapovalov, Q. M. Ramasse, K. A. Hunnestad, S. M. Selbach, U. Aschauer, K. Moore, J. M. Gregg, U. Bangert, M. Stengel, A. Gruverman, and D. Meier, arXiv:2309.02068.

[32] R. Viennois, I. Kityk, A. Majchrowski, J. Zmija, Z. Mierczyk, and P. Papet, Mater. Chem. Phys. **213**, 461 (2018).

[33] M. Fava, W. Lafargue-Dit-Hauret, A. H. Romero, and E. Bousquet, Phys. Rev. B **108**, L201112 (2023).

[34] K. F. Garrity, K. M. Rabe, and D. Vanderbilt, Phys. Rev. Lett. **112**, 127601 (2014).

[35] H. Zabrodsky and D. Avnir, J. Am. Chem. Soc. **117**, 462 (1995).

[36] K. Ishito, H. Mao, Y. Kousaka, Y. Togawa, S. Iwasaki, T. Zhang, S. Murakami, J.-i. Kishine, and T. Satoh, Nat. Phys. **19**, 35 (2023).

[37] H. Ueda, M. García-Fernández, S. Agrestini, C. P. Romao, J. van den Brink, N. A. Spaldin, K.-J. Zhou, and U. Staub, Nature (London) **618**, 946 (2023).

[38] X. Gonze, F. Jollet, F. Abreu Araujo, D. Adams, B. Amadon, T. Applencourt, C. Audouze, J.-M. Beuken, J. Bieder, A. Bokhanchuk, E. Bousquet, F. Bruneval, D. Caliste, M. Côté, F. Dahm, F. Da Pieve, M. Delaveau, M. Di Gennaro, B. Dorado, C. Espejo *et al.*, Comput. Phys. Commun. **205**, 106 (2016).

[39] X. Gonze, B. Amadon, G. Antonius, F. Arnardi, L. Baguet, J.-M. Beuken, J. Bieder, F. Bottin, J. Bouchet, E. Bousquet, N. Brouwer, F. Bruneval, G. Brunin, T. Cavignac, J.-B. Charraud, W. Chen, M. Côté, S. Cottenier, J. Denier, G. Geneste *et al.*, Comput. Phys. Commun. **248**, 107042 (2020).

[40] M. J. van Setten, M. Giantomassi, E. Bousquet, M. J. Verstraete, D. R. Hamann, X. Gonze, and G.-M. Rignanese, Comput. Phys. Commun. **226**, 39 (2018).

[41] J. P. Perdew, K. Burke, and M. Ernzerhof, Phys. Rev. Lett. **77**, 3865 (1996).

[42] X. Gonze and C. Lee, Phys. Rev. B **55**, 10355 (1997).

[43] R. D. King-Smith and D. Vanderbilt, Phys. Rev. B **47**, 1651 (1993).

[44] N. A. Spaldin, J. Solid State Chem. **195**, 2 (2012).

[45] See Supplemental Material at http://link.aps.org/supplemental/10.1103/PhysRevB.109.024113 for additional information concerning the paraelectric linear responses, interatomic force constants, phonon angular momentum, the fitting of the energy model and the hyperferroelectricity.

[46] D. Orobengoa, C. Capillas, M. I. Aroyo, and J. M. Perez-Mato, J. Appl. Crystallogr. **42**, 820 (2009).

[47] J. Hlinka, J. Privratska, P. Ondrejkovic, and V. Janovec, Phys. Rev. Lett. **116**, 177602 (2016).

[48] T. Hayashida, Y. Uemura, K. Kimura, S. Matsuoka, D. Morikawa, S. Hirose, K. Tsuda, T. Hasegawa, and T. Kimura, Nat. Commun. **11**, 4582 (2020).

[49] P. Ghosez, X. Gonze, and J.-P. Michenaud, Europhys. Lett. **33**, 713 (1996).

[50] E. Bousquet and P. Ghosez, Phys. Rev. B **74**, 180101(R) (2006).

[51] P. Li, X. Ren, G.-C. Guo, and L. He, Sci. Rep. **6**, 34085 (2016).

[52] M. Khedidji, D. Amoroso, and H. Djani, Phys. Rev. B **103**, 014116 (2021).

[53] K. D. Hammonds, M. T. Dove, A. P. Giddy, V. Heine, and B. Winkler, Am. Mineral. **81**, 1057 (1996).

[54] A. C. Garcia-Castro, N. A. Spaldin, A. H. Romero, and E. Bousquet, Phys. Rev. B **89**, 104107 (2014).

[55] W. Cochran, Phys. Rev. Lett. **3**, 412 (1959).

[56] G. Burns and B. Scott, Phys. Lett. A **39**, 177 (1972).

[57] J. F. Ryan and K. Hisano, J. Phys. C: Solid State Phys. **6**, 566 (1973).

[58] T. J. Hosea, D. J. Lockwood, and W. Taylor, J. Phys. C: Solid State Phys. **12**, 387 (1979).

[59] S. Satija and R. A. Cowley, Phys. Rev. B **25**, 6765 (1982).

[60] Y. Shen, J. Cai, H.-C. Ding, X.-W. Shen, Y.-W. Fang, W.-Y. Tong, X.-G. Wan, Q. Zhao, and C.-G. Duan, Adv. Theory Simul. **2**, 1900029 (2019).
[61] X. Cheng, J. Yuan, X. Zhu, K. Yang, M. Liu, and Z. Qi, J. Phys. D: Appl. Phys. **51**, 095303 (2018).
[62] S. Qiu, S. Rhodes, and H. Fu, Phys. Rev. B **107**, 094108 (2023).
[63] R. Adhikari and H. Fu, Phys. Rev. B **99**, 104101 (2019).
[64] S. Liu and R. E. Cohen, J. Phys.: Condens. Matter **29**, 244003 (2017).
[65] Y. Iwata, J. Phys. Soc. Jpn. **43**, 961 (1977).
[66] J. H. J. Hatano, T. K. T. Kojima, Y. M. Y. Matsui, Y. I. Y. Ishida, H. U. H. Uehara, K. T. K. Takahashi, and Y. A. Y. Adachi, Jpn. J. Appl. Phys. **36**, 6155 (1997).
[67] W. Zhong, R. D. King-Smith, and D. Vanderbilt, Phys. Rev. Lett. **72**, 3618 (1994).
[68] A. Subedi, Phys. Rev. B **92**, 214303 (2015).
[69] R. Mankowsky, A. von Hoegen, M. Först, and A. Cavalleri, Phys. Rev. Lett. **118**, 197601 (2017).
[70] P. Chen, C. Paillard, H. J. Zhao, J. Íñiguez, and L. Bellaiche, Nat. Commun. **13**, 2566 (2022).
[71] G. H. Fecher, J. Kübler, and C. Felser, Materials **15**, 5812 (2022).
[72] L. Zhang and Q. Niu, Phys. Rev. Lett. **115**, 115502 (2015).
[73] D. M. Juraschek and N. A. Spaldin, Phys. Rev. Mater. **3**, 064405 (2019).
[74] L. Zhang and Q. Niu, Phys. Rev. Lett. **112**, 085503 (2014).
[75] X. Wu and D. Vanderbilt, Phys. Rev. B **73**, 020103(R) (2006).
[76] M. Y. Gureev, A. K. Tagantsev, and N. Setter, Phys. Rev. B **83**, 184104 (2011).
[77] M. Först, C. Manzoni, S. Kaiser, Y. Tomioka, Y. Tokura, R. Merlin, and A. Cavalleri, Nat. Phys. **7**, 854 (2011).
[78] A. Zabalo and M. Stengel, Phys. Rev. Lett. **131**, 086902 (2023).